RSC Advances

PAPER

View Article Online
View Journal | View Issue

Cite this: *RSC Adv.*, 2021, **11**, 16201

Preparation, characterization serpentine-loaded hydroxyapatite and its simultaneous removal performance for fluoride, iron and manganese

Xilin Li, *[a] Xiaowan Yu,[a] Ling Liu,[a] Jianlin Yang,[b] Siyuan Liu[a] and Tianyi Zhang[a]

Aiming at the problem of excessive fluorine, iron, and manganese pollution in groundwater in mining areas, a serpentine-loaded hydroxyapatite (Srp/HAP) composite adsorbent was prepared by wet chemical coprecipitation. The preparation conditions of the Srp/HAP composite adsorbent were explored, Srp/HAP was microscopically characterized, and the adsorption performance and adsorption mechanism of the Srp/HAP composite adsorbent for F^-, Fe^{2+} and Mn^{2+} were analyzed. The results showed that the optimal preparation conditions for the composite particles were as follows: solid–liquid ratio of Srp to calcium nitrate solution 20%, aging time 20 h, calcination temperature 180 °C, and calcination time 90 min. Compact Srp/HAP composite adsorbent particles were successfully prepared, and both the lamellar crimp structure of the Srp surface and the problem of HAP surface agglomeration were resolved. After loading, the specific surface area and pore volume of the particles significantly increased, and the surface pore structure improved, which is conducive to the simultaneous adsorption and removal of fluorine, iron and manganese. The optimal reaction conditions for Srp/HAP treatment of composite water samples with F^-, Fe^{2+} and Mn^{2+} mass concentrations of 5 mg L^{-1}, 20 mg L^{-1} and 5 mg L^{-1}, respectively, are as follows: dosage of Srp/HAP 3 g L^{-1}, pH 7, temperature 35 °C, and reaction time 150 min. Under these conditions, the removal rates of F^-, Fe^{2+} and Mn^{2+} were 98.6%, 99.9% and 99.8%, respectively. The quasi-second-order kinetic model and Langmuir isothermal adsorption model described the adsorption process of F^-, Fe^{2+} and Mn^{2+} by the composite particles well. The adsorption process includes both surface physical adsorption and chemical adsorption. Chemical adsorption is mainly characterized by ion exchange and surface complexation. The Srp/HAP composite particles can be used as an excellent adsorbent for the treatment of groundwater containing fluorine, iron and manganese ions in mining areas.

Received 14th March 2021
Accepted 26th April 2021

DOI: 10.1039/d1ra02028e

rsc.li/rsc-advances

1. Introduction

The gradual advancement of global industrialization and urbanization has led to the pollution of groundwater and other natural resources. Many countries and regions, including China, India, Africa, Latin America, Europe, the United States, and the Middle East, also have problems with excessive fluorine, iron, and manganese in groundwater, seriously affecting the health and quality of life of residents.[1] Problems related to high fluorine, iron and manganese concentrations in groundwater have been reported in northeastern China, northern Shaanxi, central and northern Inner Mongolia.[2,3] Fluorine is one of the trace elements required by the human body. A small amount of fluorine is absorbed to enhance bone hardness, but excessive intake can cause bone fluorosis, which can even be life-threatening in severe cases.[4] Iron is an essential trace element for the human body. Iron ions participate in the transport of oxygen required by the human body. Iron deficiency can reduce the body's immune function. However, excessive iron ions will accumulate in the human body, causing irreversible damage.[5] Manganese ions are involved in the development of human bones, the reproductive system and the brain. But long-term exposure to a high-manganese environment will affect the central nervous system, resulting in severe mental disorders.[6] If groundwater with high fluoride, iron and manganese concentrations is used as the source of drinking water for a long time, it will seriously affect human health and cause irreversible harm to the human body.[7,8]

There are many studies on the treatment of groundwater containing fluorine at home and abroad, and many scholars have conducted studies on groundwater containing excess iron and manganese.[9–11] However, there are few studies on simultaneous removal when these three ions coexist, so it is necessary to combine groundwater fluoride removal with the removal of iron and manganese.[12] Compared with other contaminant

[a]*School of Civil Engineering, Liaoning Technical University, No. 88 Yulong Road, Fuxin, Liaoning Province 123000, China. E-mail: lixilin@lntu.edu.cn*
[b]*School of Materials Science and Engineering, Liaoning Technical University, No. 47 Zhonghua Road, Fuxin, Liaoning Province 123000, China*

treatment methods in groundwater, adsorption has the advantages of low cost and environmental friendliness and has become a popular method for fluoride and manganese removal. The selection and preparation of adsorbents for simultaneous fluoride and manganese removal are key to research and applications.[13] Natural minerals with a low price and good chemical stability, such as zeolite, sepiolite, tourmaline, and hydroxyapatite (HAP), are often used to adsorb and treat heavy metal ions in water.[14–18] HAP is a natural apatite mineral. At the beginning of the 20th century, Suzuki *et al.*,[19] a Japanese group, used HAP as an adsorbent for the first time to treat Pb^{2+}, Cd^{2+} and Cu^{2+} polluted wastewater and found that HAP had a good adsorption capacity for these ions. Later, a large number of scholars carried out studies on the adsorption, removal process and removal ability of HAP for heavy metal ions.[20] However, HAP alone has disadvantages such as a small adsorption capacity, easy blockage of adsorbent channels, difficult separation from water, and a small effective pH range.[21] At present, the commonly used HAP modification technologies are pore expansion, granulation, doping, and surface modification, which are relatively complex.[22–24] Ersan *et al.*[25] adsorbed tetracycline with a composite of kaolin and HAP. Liu *et al.*[26] reported that coating HAP particles with attapulgite improved the removal efficiency of Cd by HAP. The study showed that when powdered HAP adsorbs pollutants, it tends to clump together and cause agglomeration. Choosing a appropriate carrier can effectively reduce the agglomeration between particles and improve the adsorption performance of HAP. Srp contains a large number of hydroxyl groups, unsaturated Si–O–Si and O–Si–O bonds, magnesium-containing bonds and hydrogen bonds, so it has strong ion exchange performance. It can undergo adsorption and surface coordination reactions with many metal ions or metal ion hydroxyl complexes and is an excellent carrier.[27]

Based on the above, a new serpentine-loaded hydroxyapatite (Srp/HAP) composite adsorbent with low cost and good adsorption effect was optimized and synthesized by a wet chemical coprecipitation method using the advantages of Srp and HAP. The Brunauer–Emmett–Teller (BET) method was used to determine the specific surface area, and X-ray diffraction (XRD), scanning electron microscopy (SEM), energy dispersive X-ray spectroscopy (EDS), and Fourier transform infrared spectroscopy (FTIR) were used to further characterize the Srp/HAP composite. Moreover, the simultaneous adsorption effect for F^-, Fe^{2+}, and Mn^{2+} was studied to provide a reference for the application of Srp/HAP composite adsorbents in the treatment of groundwater used as a drinking water source and the remediation of groundwater pollution in mining areas.

2. Materials and methods

2.1 Material preparation

Srp was obtained from the Dashiqiao Houxianyu boron mining area in Yingkou City, Liaoning Province. HAP-loaded Srp was prepared by the wet chemical coprecipitation method.[28] Srp (120 mesh) was uniformly dispersed in calcium nitrate solution (0.5 mol L^{-1}) at a certain solid–liquid ratio. After stirring for 6 h, 1 mol L^{-1} phosphoric acid solution (controlled Ca/P molar ratio of 1.67) was slowly dropped into the solution to form a gel. After aging for a certain time (to effectively release basicity from Srp to reduce the amount of ammonia required), ammonia was added to adjust the pH to 11, and then aging was performed again for 24 h. After filtration, the filter cake was dried in the oven at 90 °C for 72 h to form a dry gel. This gel was then calcined at 400 °C (in a previous study, the calcination temperature for preparing HAP alone was 400 °C) for 60 min in a muffle furnace and ground through a 120 mesh sieve. The temperature was adjusted to 80 °C, 2% gelatinized etherified starch was added to make 3–5 mm particles, and the sample was calcined at a certain temperature for a certain time to prepare the composite particle adsorbent (Fig. 1). All chemical reagents used were of analytical grade and purchased from Quanrui Reagent Co., Ltd. (Liaoning, China).

2.2 Characterization of materials

The specific surface area and pore size distribution of the adsorbent were analyzed by the N_2 adsorption–desorption method with a Kangta Autosorb-iQ surface and porosity analyzer. A Shimadzu XRD-6100 X-ray diffractometer was used for phase analysis of the samples. A JSM-7500F scanning electron microscope (Japan) was used to analyze the surface morphology changes, particle size and agglomeration of the material. An FYFS-2002E EDS detector was used to characterize the surface morphology and chemical element types of the composites. An IRPrestige-21 FTIR spectrometer was used to characterize the molecular structure, chemical bond and functional group changes of the adsorbents.

2.3 Adsorption experiment

The region under study was Fuxin City, Liaoning Province, which is a typical high-fluorine, high-iron and high-manganese region in China. Considering the volatility and complexity of the actual groundwater, simulated water samples were prepared to model the groundwater quality in the Fuxin mining area. The concentrations of F^-, Fe^{2+} and Mn^{2+} in the water samples were 5 mg L^{-1}, 20 mg L^{-1} and 5 mg L^{-1}, respectively, and the pH was adjusted to 6.5. Sodium fluoride (NaF, analytically pure), ferrous sulfate ($FeSO_4 \cdot 7H_2O$, analytically pure), manganese sulfate ($MnSO_4 \cdot H_2O$, analytically pure) were purchased from Quanrui

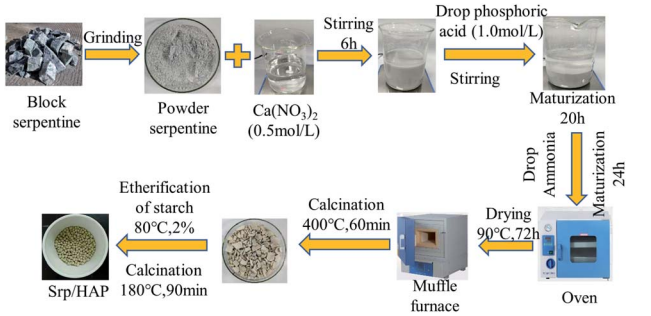

Fig. 1 Preparation of Srp/HAP composite particles.

Reagent Co., Ltd. (Liaoning, China). F^- was determined by a PF-2-01 fluoride ion selective electrode, Fe^{2+} and Mn^{2+} were determined by a Z-2000 atomic absorption spectrophotometer, and pH was determined by a PHS-3C precision pH meter.

In the preliminary experiment, the effects of the solid–liquid ratio of Srp to calcium nitrate solution, aging time, calcination temperature and calcination time on adsorption by Srp/HAP were investigated. In the static adsorption experiment, the effects of dosage, pH value, reaction temperature, reaction time and heavy metal concentration on the adsorption properties of F^-, Fe^{2+} and Mn^{2+} were investigated. In the adsorption kinetics experiment, the ranges of F^-, Fe^{2+} and Mn^{2+} were 5–20 mg L^{-1}, 20–40 mg L^{-1}, and 5–20 mg L^{-1}, respectively, and the adsorption time range was 1–150 min. In the isothermal adsorption test, the ranges of F^-, Fe^{2+} and Mn^{2+} ions in the test water samples were controlled at 5–50 mg L^{-1}, 20–100 mg L^{-1} and 5–50 mg L^{-1}, respectively, under the optimal static test conditions, and the adsorption isothermal reaction was carried out at 25 °C, 30 °C and 35 °C. The specific experimental steps were as follows: 150 mL of a composite test water sample was added to a 250 mL Erlenmeyer flask; an appropriate amount of Srp/HAP was added; and the sample was placed in a constant-temperature shaker and oscillated at 150 rad min^{-1}. After the reaction, the concentrations of F^-, Fe^{2+} and Mn^{2+} and pH were measured. The adsorption capacity per unit mass of Srp/HAP for F^-, Fe^{2+} and Mn^{2+} and the removal rate of heavy metal ions R (%) were calculated using the following formulas:

$$q_e = \frac{\Delta C_0 - C_e \Delta V}{m} \quad (1)$$

$$R = \frac{C_0 - C_e}{C_0} \times 100\% \quad (2)$$

where q_e—adsorption capacity at equilibrium, mg g^{-1}; C_0—initial concentration of solution, mg L^{-1}; C_e—concentration of solution at adsorption equilibrium, mg L^{-1}; V—volume of solution, L; and m—mass of adsorbent, g.

2.4 Desorption and regeneration

In order to regenerate Srp/HAP that was contaminated with the adsorbed F^-, Fe^{2+} and Mn^{2+} after the groundwater treatment process, these ions were desorption using batch experiments. The contaminated Srp/HAP was separated from the treatment media by filtration after adsorption, and washed with deionized water to remove any unabsorbed F^-, Fe^{2+}, and Mn^{2+}. The desorption studies were carried out by adding contaminated Srp/HAP into 0.1 M Na_2CO_3 solution, and the mixture was shaken for 150 min at 35 °C and 150 rpm. Subsequently, Srp/HAP was washed with deionized water to remove Na_2CO_3 on the surface. Then, Srp/HAP into 0.1 M HNO_3 solution again, and the mixture was shaken for 150 min at 35 °C and 150 rpm. Subsequently, Srp/HAP was washed with deionized water to remove HNO_3 on the surface. Finally dried at 110 °C for 2 h. Adsorption–desorption cycle test repeated 5 times and the F^-, Fe^{2+}, and Mn^{2+} concentration in the process was measured and recorded.

3. Results and discussion

3.1 Preparation of Srp/HAP

3.1.1 Effect of the solid–liquid ratio of Srp to calcium nitrate solution. The aging time, calcination temperature, and calcination time were fixed at 12 h, 150 °C, and 60 min, respectively, and Srp-to-calcium nitrate solution solid–liquid ratios of 10%, 20%, 40%, 60%, 80%, 100% were used to prepare Srp/HAP. The effect of the solid–liquid ratio of Srp to calcium nitrate solution on the adsorption capacity of the resulting

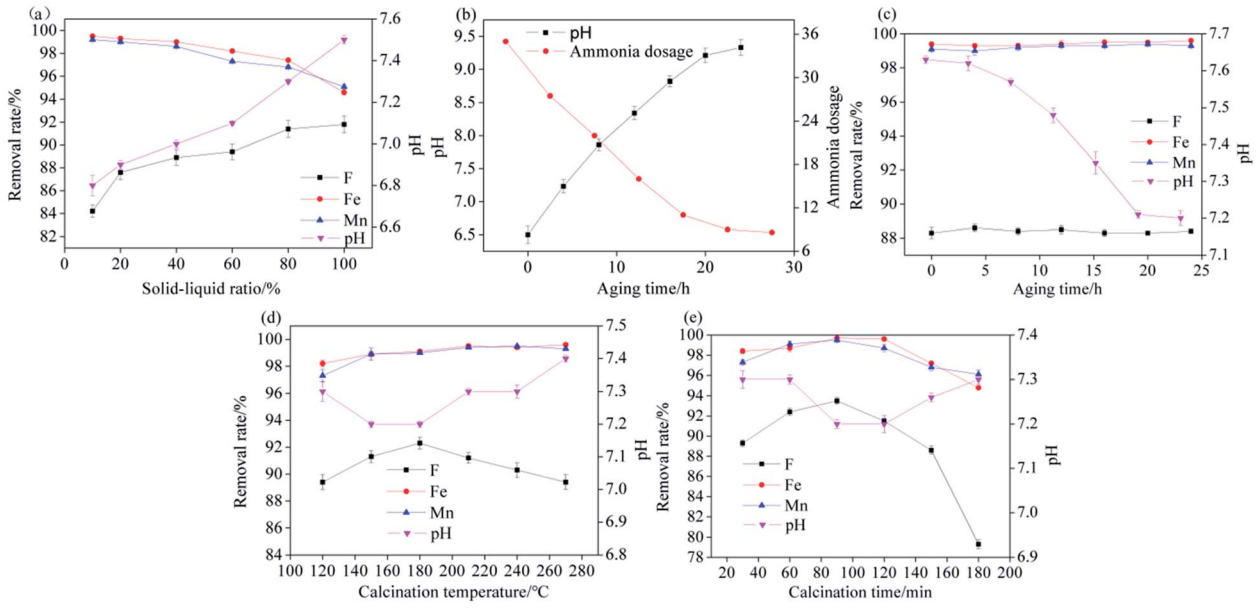

Fig. 2 Preparation of Srp/HAP (effect of different preparation conditions on Srp/HAP of (a) solid–liquid ratios, (b) pH, (c) aging times, (d) calcination temperatures, (e) calcination times, respectively).

composites for F^-, Fe^{2+} and Mn^{2+} ions under a Srp/HAP dosage of 3.33 g L^{-1}, pH of 6.5, reaction time of 120 min, and reaction temperature of 25 °C is shown in Fig. 2(a). As the solid-to-liquid ratio of Srp to calcium nitrate solution gradually increased, the removal rate of F^- from the test water sample by the synthesized Srp/HAP gradually increased, and the removal rates of Fe^{2+} and Mn^{2+} ions decreased. This is consistent with the results of the previous experiments of our research group, Srp has a higher removal rate of F^- than HAP, and a lower removal rate of Fe^{2+}, Mn^{2+} than HAP.[29] After the reaction, the pH of the test water sample increased compared to the original pH, and the increase in pH was greater with an increased amount of Srp. When the solid–liquid ratio increased from 10% to 100%, the pH of the solution increased in a small range, from 6.8 to 7.5 after the reaction. This effect was due to the release of OH^- alkalinity from the Srp into the water. On the basis of comprehensive comparison, the best simultaneous removal of fluoride, iron and manganese by Srp/HAP was achieved when a solid–liquid ratio of 20% was used for the synthesis of Srp/HAP. Under this condition, the removal rates of F^-, Fe^{2+} and Mn^{2+} were 87.6%, 99.3%, and 99%, respectively, and the pH of the solution after the reaction was 6.9.

3.1.2 Influence of aging time. The solid–liquid ratio of Srp to calcium nitrate solution, calcination temperature, and calcination time were fixed at 20%, 150 °C, and 60 min, respectively, and aging times of 0 h, 4 h, 8 h, 12 h, 16 h, 20 h, and 24 h were used to prepare Srp/HAP. The adsorption capacity for F^-, Fe^{2+} and Mn^{2+} ions by Srp/HAP at a dosage of 3.33 g L^{-1}, pH of 6.5, reaction time of 120 min, and reaction temperature of 25 °C are shown in Fig. 2(b) and (c). As shown in Fig. 2(b), the initial pH of the mixture of calcium nitrate solution and Srp was 6.5. With prolonged aging time, Srp gradually released alkalinity in the form of OH^-, making the pH of the mixed solution gradually increase. After aging for 24 h, the pH increased to a maximum of 9.33, and the amount of ammonium hydroxide (analytically pure) needed to adjust the pH to 11 decreased from 35 mL to 8.6 mL. As shown in Fig. 2(c), the use of different aging times in Srp/HAP synthesis had little effect on the removal of F^-, Fe^{2+} and Mn^{2+} in the test water samples. With prolonged aging time, the pH of the solution after the reaction gradually decreased. When the aging time was 20 h, the pH of the solution stabilized at 7.2 after Srp/HAP treatment. In summary, in the process of preparing Srp/HAP, the optimal aging time for the mixed solution of Srp and calcium nitrate before adding ammonia to adjust the pH was 20 h. Under this condition, the amount of ammonia needed to synthesize Srp/HAP was 11 mL, which was 2/3 less than the amount of ammonia required without aging. The removal rates of F^-, Fe^{2+} and Mn^{2+} by the synthesized Srp/HAP were 88.3%, 99.5%, and 99.3%, respectively, and the pH of the test water sample after the reaction was 7.2.

Table 1 BET analysis results for Srp, HAP and Srp/HAP

Sample	Average pore volume/cm^3 g^{-1}	Average pore size/nm	Specific surface area/m^2 g^{-1}
Srp/HAP	0.139	13.18	42.10
Srp	0.0019	19.06	5.35
HAP	0.0095	5.08	21.68

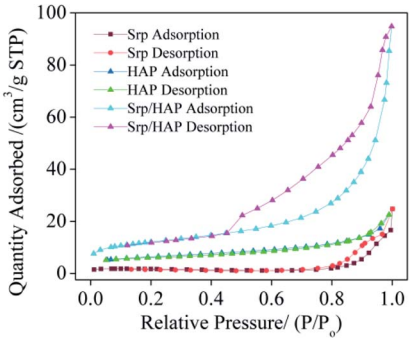

Fig. 3 N_2 adsorption–desorption isotherms of Srp, HAP and Srp/HAP.

3.1.3 Influence of calcination temperature. The solid–liquid ratio of Srp to calcium nitrate solution, aging time, and calcination time were fixed at 20%, 20 h, and 60 min, respectively, and the calcination temperature was set to 120 °C, 150 °C, 180 °C, 210 °C, 240 °C, and 270 °C to prepare Srp/HAP. The influence of calcination temperature on the adsorption of F^-, Fe^{2+} and Mn^{2+} ions at a Srp/HAP dosage of 3.33 g L^{-1}, pH of 6.5, reaction time of 120 min, and reaction temperature of 25 °C is shown in Fig. 2(d). The removal rate of F^- reached a peak at 180 °C and the removal rates of Fe^{2+} and Mn^{2+} were basically stable after reaching maximum values at 220 °C. Changes in calcination temperature affect the crystallinity of chemical components in Srp/HAP and the consolidation degree of the composite adsorbent particles. When the calcination temperature is low or high, the dispersion rate of Srp/HAP particles will increase, making it easier for OH^- in Srp to diffuse into the water and reducing the removal rate of F^- from the test water sample. After the reaction, the pH increased, fluctuating between 7.2 and 7.4. A comprehensive comparison showed that 180 °C is the best calcination temperature for the synthesis of Srp/HAP.

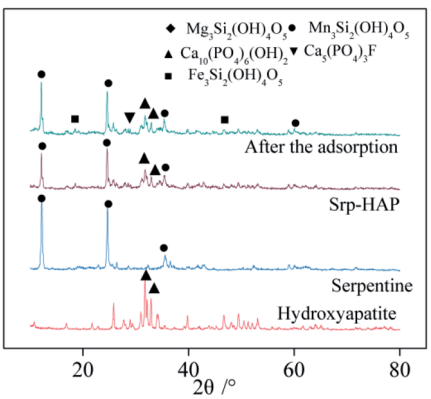

Fig. 4 XRD patterns of Srp, HAP, Srp/HAP and Srp/HAP after reaction.

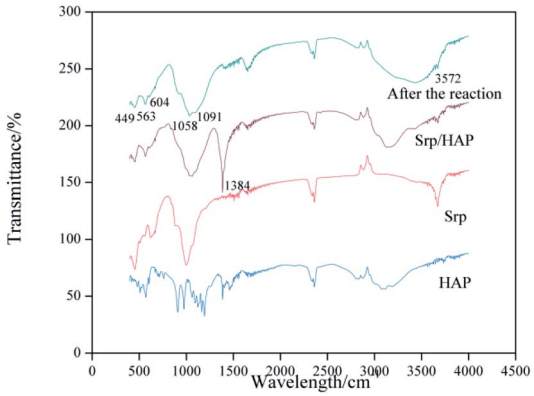

Fig. 5 FTIR spectra of Srp, HAP, and Srp/HAP.

3.1.4 Influence of calcination time. The solid–liquid ratio of Srp to calcium nitrate solution, aging time, and calcination temperature were fixed at 20%, 20 h, and 180 °C, respectively, and calcination times of 30 min, 60 min, 90 min, 120 min, 150 min, and 180 min were used to prepare Srp/HAP. The influence of calcination time on the adsorption of F^{-}, Fe^{2+} and Mn^{2+} ions at a Srp/HAP dosage of 3.33 g L^{-1}, pH of 6.5, reaction time of 120 min, and reaction temperature of 25 °C is shown in Fig. 2(e). As the calcination time increased, the removal rate of each ion first increased and then decreased, reaching a peak at 90 min. Too long a calcination time will not only destroy the crystal lattice of HAP but also make the HAP particles coarser and reduce the specific surface area of the HAP loaded on the Srp surface, reducing the adsorption effect for each ion. The pH values of Srp/HAP samples synthesized with different calcination times were higher than the original pH values, and the overall stable value was between 7.2 and 7.3. After comprehensive comparison, 90 min was finally determined to be the optimal calcination time for preparing Srp/HAP.

3.2 Characterization of composite materials

Table 1 shows the BET analysis results for Srp, HAP and Srp/HAP composite particles. Fig. 3 shows the N_2 adsorption–desorption isotherms of Srp, HAP and Srp/HAP composite

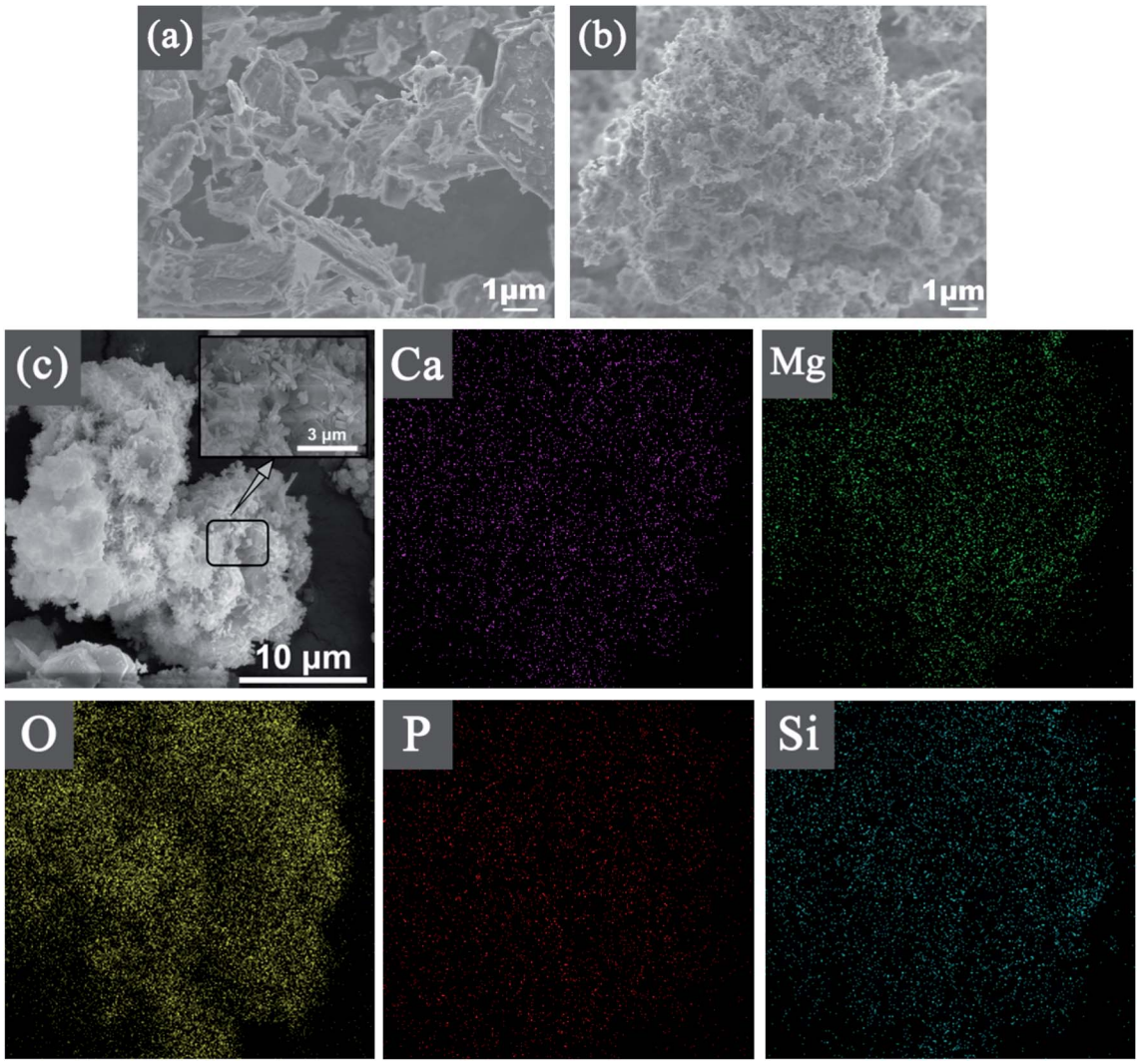

Fig. 6 SEM images of (a) Srp, (b) HAP, (c) Srp/HAP and EDS surface scanning of (c) Srp/HAP.

particles. As shown in Table 1, the BET specific surface areas of Srp, HAP and Srp/HAP composite particles were 5.35, 21.68 and 42.10 $m^2 g^{-1}$, respectively. The specific surface area of Srp/HAP was 1.9 times that of HAP and 7.9 times that of Srp. Fig. 3 shows that the adsorption–desorption isotherms of Srp, HAP and Srp/HAP composite particles are all typical Langmuir II mesoporous material adsorption curves. Since the larger the specific surface area of the adsorbent is, the more adsorption sites are available on its surface, the Srp/HAP composite particles were more conducive than their individual components to the adsorption of F^-, Fe^{2+} and Mn^{2+} ions.

Fig. 4 shows the XRD patterns of Srp, HAP, Srp/HAP and Srp/HAP after adsorption. Fig. 4 shows that the composite particles are mainly composed of $Ca_{10}(PO_4)_6(OH)_2$ from HAP and $Mg_3Si_2(OH)_4O_5$ from Srp. Srp/HAP mainly had five characteristic peaks (at 2θ of 12.12°, 25.76°, 32.92°, 33.96°, and 35.40°). However, the peaks of Srp and HAP in the composite particles were relatively weak, which may be because the loading process of HAP on the surface of Srp made the contents of Srp and HAP lower than those in the single substances[30] or because the HAP partially covered the Srp.[31] A new characteristic peak appeared in the XRD pattern of the water sample after adsorption by Srp/HAP composite particles. XRD analysis showed that the adsorbed materials formed $Fe_3Si_2(OH)_4O_5$, $Mn_3Si_2(OH)_4O_5$ and $Ca_5(PO_4)_3F$ compounds. The F^- in the test water sample and the OH^- in $Ca_{10}(PO_4)_6(OH)_2$; Fe^{2+} and Mg^{2+}; and Mn^{2+} in $Mg_3Si_2(OH)_4O_5$ and Mg^{2+} in $Mg_3Si_2(OH)_4O_5$ undergo ion exchange reactions to form the detected compounds. The main reactions of the three new compounds are as follows:

$$2F^- + Ca_{10}(PO_4)_6(OH)_2 \rightarrow 2Ca_5(PO_4)_3F + 2OH^- \quad (3)$$

$$3Fe^{2+} + Mg_3Si_2(OH)_4O_5 \rightarrow Fe_3Si_2(OH)_4O_5 + 3Mg^{2+} \quad (4)$$

$$3Mn^{2+} + Mg_3Si_2(OH)_4O_5 \rightarrow Mn_3Si_2(OH)_4O_5 + 3Mg^{2+} \quad (5)$$

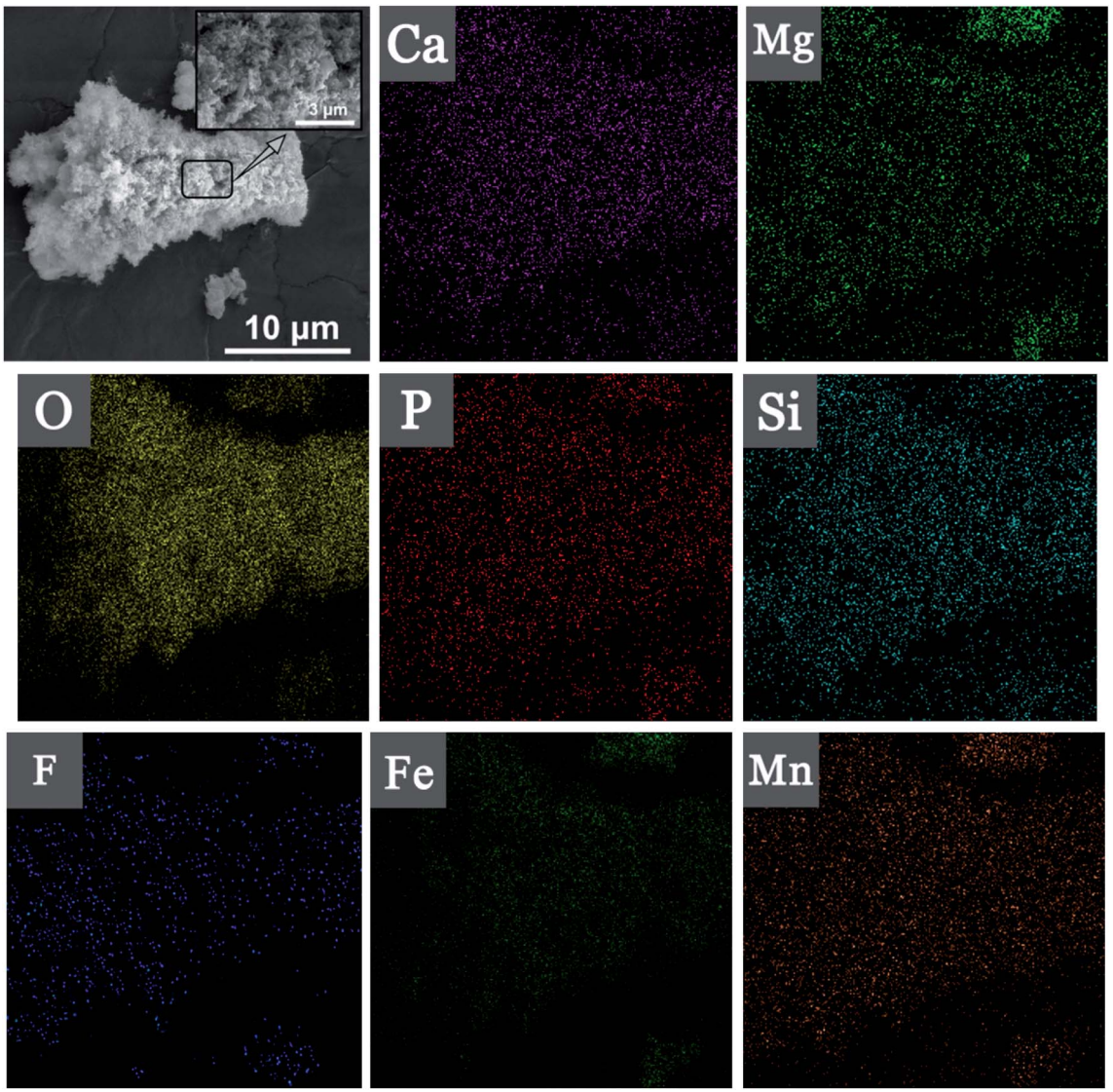

Fig. 7 SEM image and EDS surface scanning of Srp/HAP after reaction.

Table 2 Element composition and weight percentage ratio of EDS surface scanning of Srp/HAP before and after reaction

Element	Before (weight/%)	After (weight/%)
Ca	3.49	1.85
Mg	15.96	12.67
P	1.68	1.18
O	65.72	60.30
Si	13.15	8.89
F	—	2.66
Fe	—	7.03
Mn	—	5.42

Fig. 5 shows the infrared spectra of Srp, HAP and Srp/HAP composite particles. The vibration peaks of the Srp/HAP composite particles at wavelengths of 449 cm^{-1}, 563 cm^{-1}, 1058 cm^{-1} and 1091 cm^{-1} are attributed to O–Mg, P═O, P–O and Si–O, respectively. The characteristic peaks at 604 cm^{-1} and 3572 cm^{-1} are the bending and stretching vibration peaks of OH^-, respectively. All the above absorption peaks were consistent with the standard peaks of Srp and HAP in the literature,[32,33] indicating that the Srp/HAP composite was successfully prepared. The absorption peak of O–P–O at 563 cm^{-1} weakened after the reaction. It may be that the PO_4^{3-} produced by dissolution underwent a surface complex reaction with Fe^{2+} and Mn^{2+} to form phosphate complexes. Liu *et al.*[26] obtained similar conclusions when studying the adsorption of Cd^{2+} in water by HAP/bentonite composite adsorbents.

Fig. 6 shows SEM images of Srp, HAP, Srp/HAP. Fig. 6(a) shows that the surface of Srp has a superimposed lamellar porous curled structure with obvious textures and obvious concave–convex structures between the textures, indicating that Srp has a large specific surface area, which makes it have a strong physical adsorption capacity. Fig. 6(b) shows extensive particle agglomeration on the surface of HAP and an uneven pore distribution. Fig. 6(c) shows that the Srp/HAP composite adsorbent not only has the sheet-like structure of Srp surface, but also solves the problem of agglomeration on the surface of HAP. The rod-shaped micron-sized HAP clusters are uniformly distributed on the surface of Srp. The clusters are formed *via* the cross-stacking of rod-shaped HAP with a diameter of 50–100 nm and a length of 0.5–3 um. The clusters increase the surface areas and the number of surface pores, which are beneficial to the adsorption of F^-, Fe^{2+} and Mn^{2+} ions. Fig. 7 shows that the structure and morphology of the Srp/HAP composite adsorbent changed after adsorption. There were fine flocs on the surface and the surface pores are filled. It may be that F^-, Fe^{2+} and Mn^{2+} ions and the Srp/HAP composite particles underwent surface physical adsorption or surface complexation reactions.[34]

EDS surface scanning of Srp/HAP before and after reaction are shown in Fig. 6(c), 7, and Table 2. It is showed that Srp/HAP contained not only O, Mg and Si from Srp but also O, P and Ca from HAP. This result indicated that Srp was successfully loaded onto HAP in the preparation of Srp-HAP by the wet chemical coprecipitation method. F, Fe, and Mn appeared in the EDS spectrum after adsorption. The weight fraction of O decreased from 65.72% before adsorption to 60.30% after adsorption, and the weight fraction of Mg decreased from

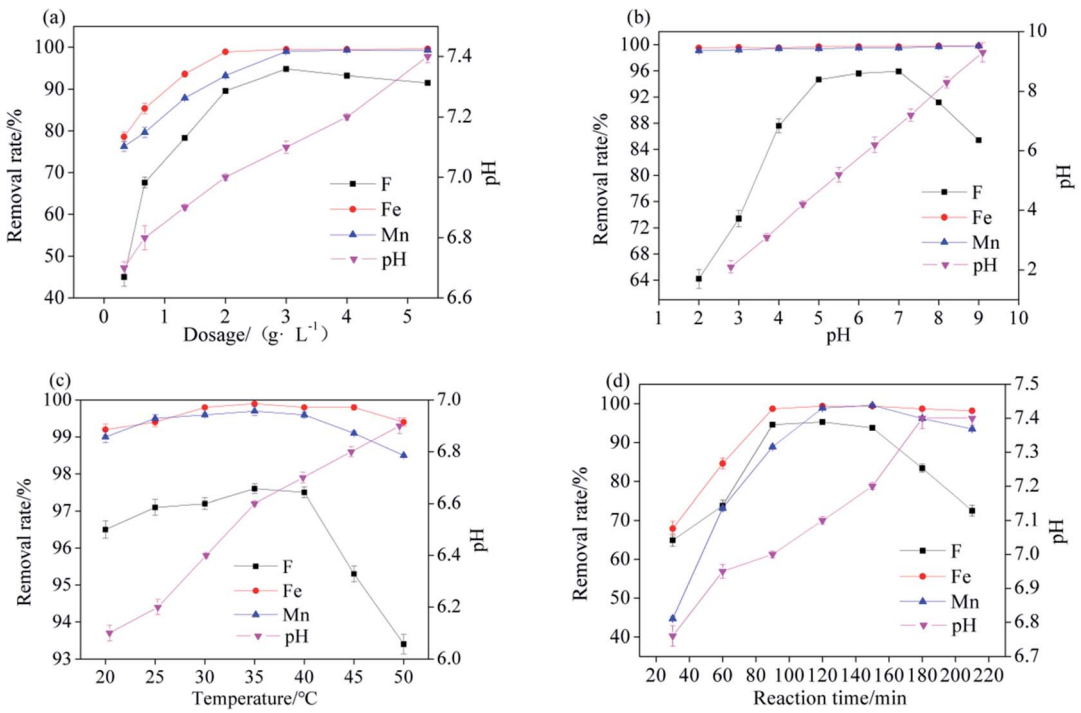

Fig. 8 Adsorption test of Srp/HAP adsorption of fluorine, iron and manganese (the adsorption of fluorine, iron and manganese by Srp/HAP of (a) dosage, (b) pH, (c) reaction temperature, (d) reaction time, respectivel).

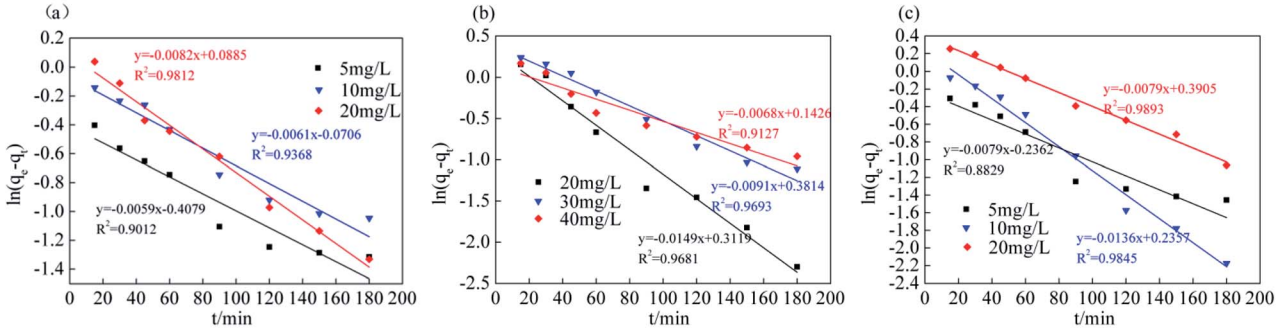

Fig. 9 Quasi-first-order kinetic equation fitting (quasi-first order kinetic equation of (a) fluoride, (b) iron, (c) manganese, respectively).

15.96% before adsorption to 12.67% after adsorption, further indicating that F^- and OH^-, Fe^{2+} and Mg^{2+}, and Mn^{2+} and Mg^{2+} may have undergone ion exchange, consistent with the XRD analysis results.

3.3 Adsorption test

3.3.1 Influence of Srp/HAP dosage. The pH, temperature, and reaction time were fixed at 6.5, 25 °C, and 120 min, respectively. The influence of Srp/HAP dosage on the adsorption capacity for F^-, Fe^{2+} and Mn^{2+} ions at Srp/HAP dosages of 0.33 g L^{-1}, 0.67 g L^{-1}, 1.33 g L^{-1}, 2 g L^{-1}, 3 g L^{-1}, 4 g L^{-1} and 5.33 g L^{-1} is shown in Fig. 8(a). When the dosage increased from 0.33 g L^{-1} to 3 g L^{-1}, the removal rate of F^- increased from 45.3% to 94.8%, and the removal rate of Mn^{2+} increased from 76.28% to 99.2%. As the dosage continued to increase, the removal rates of F^- and Mn^{2+} decreased. The maximum removal rate of Fe^{2+} was 99.4%, and was reached at a dosage of 2 g L; as the dosage continued to increase, the removal rate of Fe^{2+} remained basically stable. The greater the dose was, the higher the pH increase after the reaction. This result occurred because with increasing dosage, the OH^- content in the test water sample increased; however, if the dosage is too high, the saturated adsorbent particles will collide with each other and cause desorption. Annida *et al.*[35] used peanut shells to adsorb hexavalent chromium and found a similar conclusion. Moreover, OH^- interfered with the removal of F^- in the test water sample; at a high dosage, the removal effect of F^- was poor. On the basis of comprehensive comparison, the optimal dosage of Srp/HAP was 3 g L^{-1}.

3.3.2 Influence of pH. The Srp/HAP dosage, temperature, and reaction time were fixed at 3 g L^{-1}, 25 °C, and 120 min, respectively, and pH values of 2, 3, 4, 5, 6, 7, 8, and 9 were applied; the pH value was related to the F^-, Fe^{2+} and Mn^{2+} ion adsorption amount, as shown in Fig. 8(b). When the pH increased from 2 to 5, the F^- removal rate increased from 64.2% to 94.7%. When the pH was between 5 and 7, the F^- removal rate stabilized above 95.5%; as the pH continued to rise, the removal rate of F^- began to decrease. At low pH, H^+ combined with F^- in the test water sample to form HF; at the same time, the surface structure of the adsorbent was destroyed, and the binding ability of the adsorbent for ions was reduced. However, under alkaline conditions, the large amount of OH^- produced electrostatic repulsion to F^- and competed with F^- for active sites on the surface of the adsorbent, and the removal rate of F^- was reduced. With a gradual increase in pH, the removal rates of Fe^{2+} and Mn^{2+} by Srp-HAP intermittently increased. When the pH was greater than 5, the removal rates of Fe^{2+} and Mn^{2+} were above 99.4% and 99.7%, respectively. This result occurred because in the water environment, the OH^- content gradually increased with increasing pH, which promoted the removal of Fe^{2+} and Mn^{2+} by the adsorbent, but too high a pH caused Fe^{2+} and Mn^{2+} to precipitate and affect the turbidity of the treated water. Comprehensive comparison showed that the effective pH range for using Srp-HAP to treat the test water samples was 5–7; however, F^-, Fe^{2+} and Mn^{2+} easily accumulate in acidic

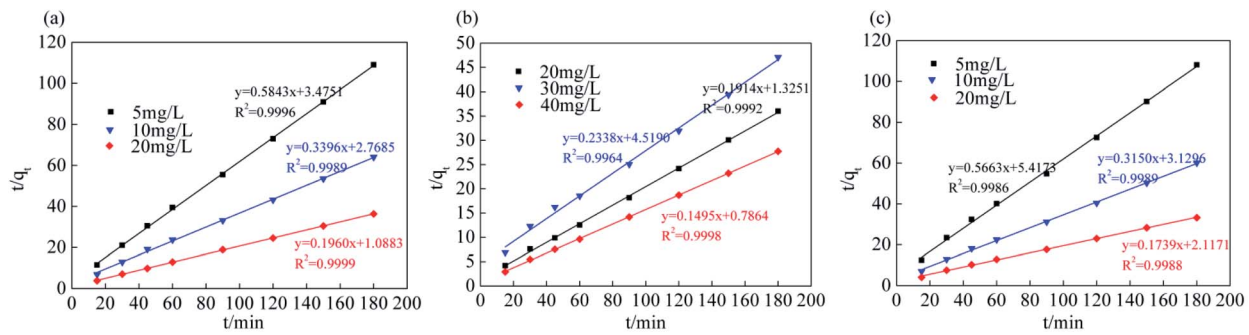

Fig. 10 Quasi second order kinetic equation fitting curve (pseudo-second-order kinetic equation of (a) fluoride, (b) iron, (c) manganese, respectively).

groundwater, and the optimal value was finally determined to be pH = 7, which corresponds to the static reaction conditions.

3.3.3 Effect of reaction temperature. The dosage of Srp/HAP, pH, and reaction time were fixed at 3 g L^{-1}, 7, and 120 min, respectively, and the reaction temperature was modified to 20 °C, 25 °C, 30 °C, 35 °C, 40 °C, 45 °C, and 50 °C. The effect on the adsorption of F^-, Fe^{2+} and Mn^{2+} ions is shown in Fig. 8(c). When the reaction temperature was between 25 °C and 40 °C, the removal rates of F^- and Fe^{2+} were basically stable at 97.5% and 99.8%, respectively. When the reaction temperature was between 30 °C and 40 °C, the removal rate of Mn^{2+} stabilized at 99.6%. When the reaction temperature was higher than 35 °C, the removal rates of F^-, Fe^{2+} and Mn^{2+} began to decrease. This increase occurred because the adsorption reaction is an exothermic reaction, and a high temperature is not conducive to the progress of the adsorption reaction. When the reaction temperature increased from 20 °C to 50 °C, the pH of the test water sample after reaction gradually increased from 6.1 to 6.9. This increase occurred because the increase in reaction temperature promoted the release of alkalinity in the form of OH^- from Srp into the water. Comprehensive analysis showed that the optimal reaction temperature for treating the water sample with Srp/HAP was 35 °C.

3.3.4 Adsorption kinetics. The quasi-first-order kinetics, quasi-second-order kinetics and particle diffusion model equations can be used to evaluate the relationship between the adsorbent adsorption amount and adsorption time. The adsorption kinetics of F^-, Fe^{2+} and Mn^{2+} on Srp/HAP were studied by the following equations:

Quasi-first-order dynamic equation:

$$\lg(q_e - q_t) = \lg(q_e) - \left(\frac{K_1}{2.303}\right)t \quad (6)$$

Quasi-second-order dynamic equation:

$$\frac{t}{q_t} = \frac{1}{K_2 {q_e}^2} + \frac{t}{q_e} \quad (7)$$

Particle diffusion model equation:

$$q_t = k_p t^{0.5} \quad (8)$$

$$k_p = \frac{6}{q_e}\sqrt{\frac{D}{\pi}} \quad (9)$$

where q_e – adsorption amount at adsorption equilibrium, mg g^{-1}; q_t – adsorption capacity at adsorption time t (min), mg g^{-1}; K_1 and K_2 – adsorption rate constants, min^{-1}; k_p – diffusion rate constant, mg g^{-1} $min^{-0.5}$; and D – particle diameter, mm.

The dosage of Srp/HAP, pH, and reaction temperature were fixed at 3 g L^{-1}, 7, and 35 °C, respectively, and the reaction time was modified to 30 min, 60 min, 90 min, 120 min, 150 min, 180 min, and 210 min. The reaction time had different effects on the F^-, Fe^{2+} and Mn^{2+} adsorption amounts, as shown in Fig. 8(d). At the initial stage of the reaction, the secondary reaction was incomplete, so the removal rates of various ions were low. When the reaction time reached 120 min, the removal rate of F^- reached a maximum of 95.3%. When the reaction proceeded to 150 min, the removal rates of Fe^{2+} and Mn^{2+} reached maximum values of 99.4% and 99.6%, respectively. At this time, the removal rate of F^- was 93.8%, and the pH of the solution was 7.2. After the reaction time exceeded 150 min, the removal rate of each ion began to decrease. This decrease occurred because the adsorption of ions by the adsorbent reached saturation, and mutual collisions caused desorption. Moreover, with prolonged reaction time, more OH^- was released from Srp to the test water sample, and the removal rate of F^- was lower. After comprehensive comparison, it was finally determined that the best response time was 150 min.

The analysis and simulation results for the quasi-first-order and quasi-second-order kinetic models are shown in Fig. 9, 10 and Table 3. The correlation coefficient for the quasi-first-order kinetic model was low, and the theoretical equilibrium adsorption capacity was quite different from the experimental results. This result occurred because quasi-first-order kinetics have limitations; the model is generally only suitable for the kinetic description of the initial stage of adsorption and cannot accurately describe the entire process of adsorption.[36] The correlation coefficient (R^2) values of the quasi-second-order kinetics model were >0.99 for all ions, and the fitted data were closer to the actual data than were the results for the quasi-first-order model. Therefore, the adsorption process of Srp/HAP for F^-, Fe^{2+} and Mn^{2+} is more in line with the quasi-second-

Table 3 Quasi-first-order and quasi-second-order kinetic fitting results

Ion type	Concentration (mg L^{-1})	Quasi-first order dynamics			Quasi-second order dynamics		
		q_e (mg g^{-1})	K_1 (min^{-1})	R^2	q_e (mg g^{-1})	K_2 (min^{-1})	R^2
F^-	5	0.6650	0.0135	0.9012	1.7114	0.0982	0.9996
	10	0.9318	0.0141	0.9368	2.9445	0.0417	0.9989
	20	1.0926	0.0189	0.9812	5.1028	0.0353	0.9999
Fe^{2+}	20	1.3660	0.0343	0.9681	5.2238	0.0277	0.9992
	30	1.4643	0.0209	0.9693	4.2775	0.0121	0.9964
	40	1.1532	0.0156	0.9127	6.6876	0.0284	0.9998
Mn^{2+}	5	0.7896	0.0182	0.8829	1.7658	0.0592	0.9986
	10	1.2657	0.0313	0.9845	3.1747	0.0317	0.9989
	20	1.4777	0.0181	0.9893	5.7494	0.0143	0.9988

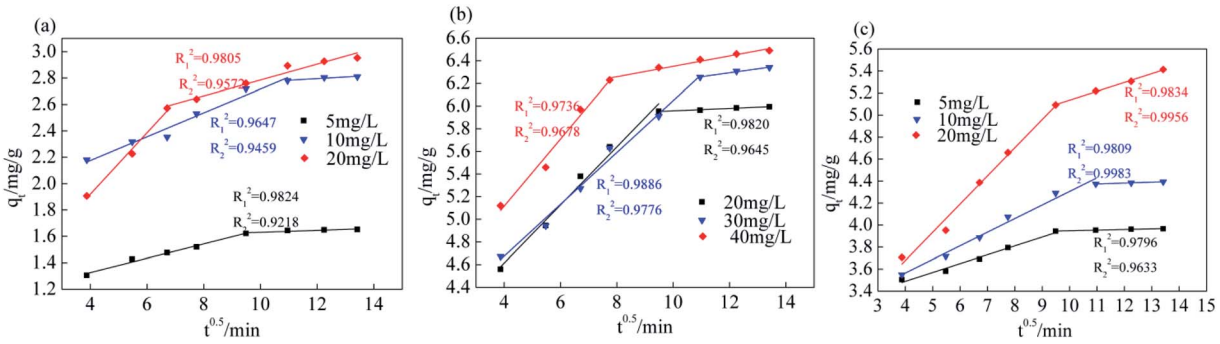

Fig. 11 Internal diffusion equation fitting curve (internal diffusion equation fitting curve of (a) fluoride, (b) iron, (c) manganese, respectively).

Table 4 Internal diffusion model fitting results

Ion type	Concentration (mg L^{-1})	K_{1d} (mg g^{-1} $min^{-0.5}$)	R_1^2	K_{2d} (mg g^{-1} $min^{-0.5}$)	R_2^2
F^-	5	0.0542	0.9824	0.0074	0.9218
	10	0.0903	0.9647	0.0123	0.9459
	20	0.2334	0.9805	0.0601	0.9572
Fe^{2+}	20	0.2567	0.9820	0.0107	0.9645
	30	0.2291	0.9886	0.0346	0.9776
	40	0.2968	0.9736	0.0460	0.9678
Mn^{2+}	5	0.0804	0.9796	0.0057	0.9633
	10	0.1235	0.9809	0.0081	0.9983
	20	0.2564	0.9834	0.0800	0.9956

order kinetic equation than the quasi-first-order kinetic equation.

From the fitting results of the internal diffusion model (Fig. 11 and Table 4), the K_{1d} value of Srp/HAP with F^-, Fe^{2+} and Mn^{2+} gradually decreases with increasing concentration, the diffusion rate of each ion on the surface of the adsorbent is proportional to the initial concentration, and the K_{1d} value is far greater than the K_{2d} value. The linear fitting results for Srp/HAP adsorption of F^-, Fe^{2+} and Mn^{2+} are segmented, and the fitting R^2 of each segment is good, indicating that the adsorption of Srp/HAP for each ion in the test water sample satisfies the internal diffusion model and each ion undergoes adsorption. The external diffusion stage occurs on the surface of the adsorbent, and in the internal diffusion stage, the ions diffuse into the adsorbent.

3.3.5 Adsorption isotherms. The Langmuir and Freundlich isotherm models were used to evaluate the adsorption mechanism of the adsorbent. The Langmuir and Freundlich isotherm model equations are as follows:

Langmuir isothermal adsorption equation:

$$\frac{c_e}{q_e} = \frac{1}{(K_L q_m)} + \frac{c_e}{q_m} \quad (10)$$

Freundlich isothermal adsorption equation:

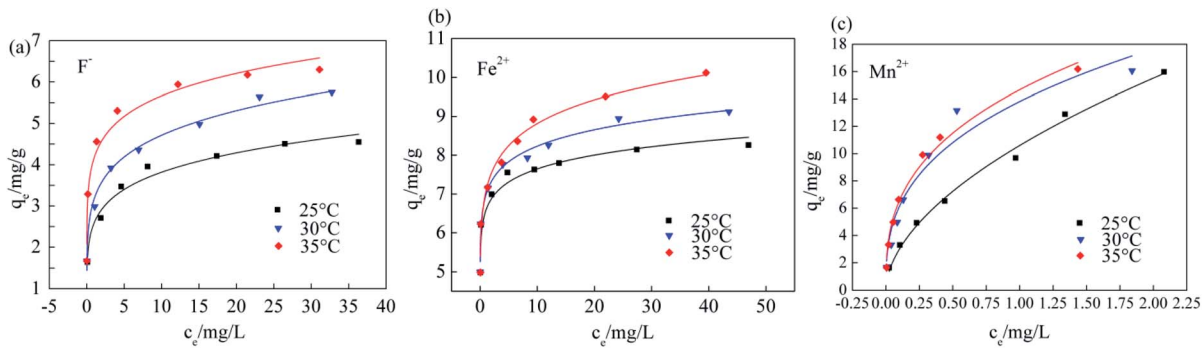

Fig. 12 Isothermal adsorption curves of Srp/HAP (effect of different heavy metal concentrations on Srp/HAP adsorption capacity of (a) fluorine, (b) iron, (c) manganese, respectively).

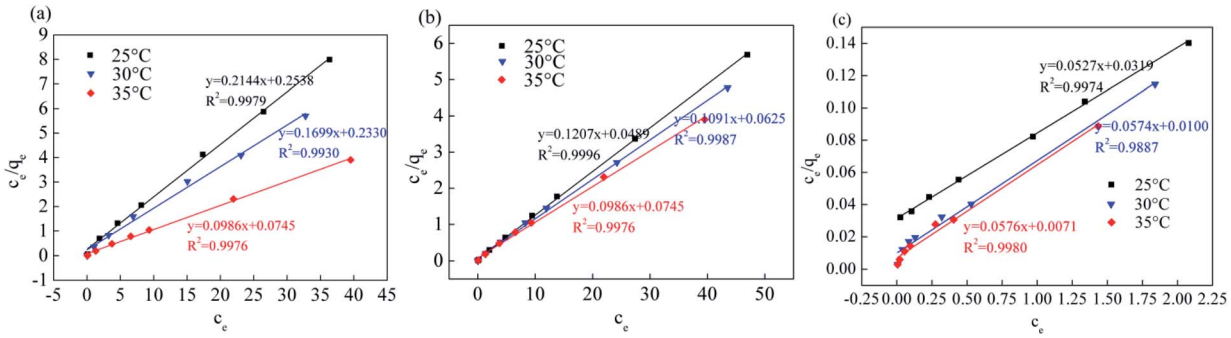

Fig. 13 Equation fitting curve of Langmuir (Langmuir equation fitting curve (a) fluorine, (b) iron, (c) manganese, respectively).

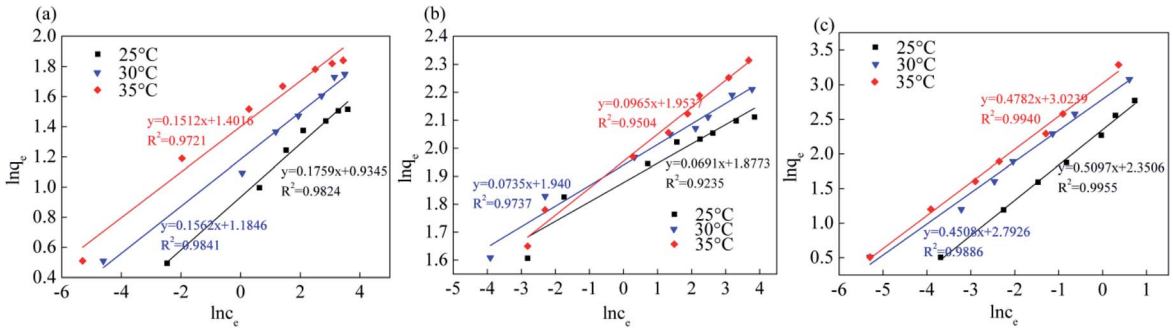

Fig. 14 Equation fitting curve of Freundlich (Freundlich equation fitting curve (a) fluorine, (b) iron, (c) manganese, respectively).

$$\ln q_e = \ln K_F + \frac{1}{n} \ln c_e \quad (11)$$

where C_e—solution concentration at adsorption equilibrium, mg L^{-1}; q_e—adsorption capacity at equilibrium, mg g^{-1}; q_m—adsorption capacity at adsorption saturation, mg g^{-1}; K_L—Langmuir constant, L mg^{-1}; and K_F—Freundlich empirical constant.

The Srp/HAP dosage, pH, reaction temperature, and reaction time were fixed at 3 g L^{-1}, 7, 35 °C, and 150 min, respectively, and the influence of different heavy metal concentrations on F^-, Fe^{2+} and Mn^{2+} adsorption was assessed as shown in Fig. 12. Fig. 12 shows that the adsorption capacity of Srp/HAP for F^-, Fe^{2+} and Mn^{2+} increased with increasing reaction temperature and concentration. Moreover, with increasing initial ion concentration, the active adsorption sites on the adsorbent surface gradually tended to become saturated, and the adsorption capacity tended to reach saturation.

Fig. 13, 14 and Table 5 show the fitting results of the Srp/HAP isotherm adsorption equations. The Langmuir correlation coefficients (R^2 > 0.98 for all ions) and Freundlich correlation coefficients (R^2 > 0.92 for all ions) indicate that both models fit the adsorption process well. However, from intuitive observation of the fitted correlation coefficients, the Langmuir isotherm model can better simulate the process of Srp/HAP adsorption of F^-, Fe^{2+} and Mn^{2+}, and the adsorption process of each ion conforms to monolayer adsorption. At 35 °C, the maximum monolayer saturated adsorption capacity Q values of

Table 5 Endothermic fitting parameters

		Langmuir			Freundlich		
Ion type	Temperature	q_m (mg g^{-1})	K_L	R^2	K_F	$1/n$	R^2
F^-	25	3.6742	0.9613	0.9979	2.2324	6.3060	0.9824
	30	5.7455	0.2889	0.9930	2.5103	5.3370	0.9841
	35	6.2406	1.0384	0.9976	3.0642	4.3439	0.9721
Fe^{2+}	25	9.2730	0.5641	0.9996	7.5073	17.7274	0.9235
	30	9.5749	0.2720	0.9989	7.7268	13.8715	0.9737
	35	11.9432	1.2350	0.9976	8.0515	14.5180	0.9504
Mn^{2+}	25	8.0985	0.5209	0.9975	4.3481	6.3175	0.9955
	30	8.2658	0.7284	0.9887	4.6410	5.9344	0.9886
	35	9.6441	0.5992	0.9980	5.1335	5.5636	0.9940

Table 6 Comparison of Srp/HAP composite adsorbent with previously reported adsorbents for the removal of fluoride, iron and manganese in terms of uptake capacity

Adsorbents	pH	q_e of F^- (mg g^{-1})	q_e of Fe^{2+} (mg g^{-1})	q_e of Mn^{2+} (mg g^{-1})	References
Natural pumice	3–11	1.17			37
Hydroxyapatite	4.16	3.12			38
Activated carbon *Moringa oleifera*	8		8.043		39
Clinoptilolite	4.6–7.0			7.69	40
Granular activated carbon	7		3.601	2.545	41
Slovakian natural zeolite	7		1.157	0.075	42
Natural shell	7.0–9.0	4.09	4.00	3.50	1
Srp/HAP	7	6.2406	11.9432	9.6441	Present work

F^-, Fe^{2+} and Mn^{2+} by Srp/HAP were 6.2406 mg g^{-1}, 11.9432 mg g^{-1}, and 9.6441 mg g^{-1}, respectively. It can be seen that the Srp/HAP adsorbent had a higher adsorption capacity than most of other adsorbents reported (Table 6). From these results, Srp/HAP could be considered as a potential efficient adsorbent for the removal of F^-, Fe^{2+} and Mn^{2+} from aqueous solution in terms of higher adsorption capacity.

3.4 Regeneration of Srp/HAP

When the adsorbent is actually used for remediation, the reuse of the adsorbent should be considered. In order to evaluate the reusability of Srp/HAP, regeneration of the used contaminated Srp/HAP adsorbent was performed in 0.1 M Na_2CO_3 and 0.1 M HNO_3 in turn. After the adsorption–desorption cycle test was repeated 5 times. The result was shown in Fig. 15. With the increase of the number of regeneration cycles, the removal rate of F^-, Fe^{2+} and Mn^{2+} by Srp/HAP gradually decreased. Compared with cycle 0, the removal rates of F^-, Fe^{2+} and Mn^{2+} decreased from 98.9%, 100%, and 99.9% to 82.1%, 89.4%, and 84.3% after 5 times regeneration (loss rate were 16.8%, 10.6%, 15.6%, respectively). This may be related to the reduction of adsorbent surface functional groups and incomplete desorption during the regeneration process, because long-term elution may destroy the binding site, or insufficient elution may leave metal ions in the adsorbent.[43] The results show that Srp/HAP has good reusability and can be used as an effective adsorption material for groundwater treatment.

3.5 Mechanism analysis

HAP was loaded on Srp to prepare Srp/HAP composite particles. From the microscopic analysis above, the Srp/HAP composite particles were composed of $Ca_{10}(PO_4)_6(OH)_2$ and $Mg_3Si_2(OH)_4O_5$. When the solution contains F^-, F^- partially replaces OH^- in $Ca_{10}(PO_4)_6(OH)_2$ and forms $Ca_{10}(PO_4)_6F_2$ on the surface of HAP.[44] The cell volume of $Ca_{10}(PO_4)_6F_2$ ($V = 523.3$) is smaller than that of $Ca_{10}(PO_4)_6(OH)_2$ ($V = 528.8$). Due to the cell mismatch, the newly formed $Ca_{10}(PO_4)_6F_2$ fell off the surface of HAP; thus, fine $Ca_{10}(PO_4)_6F_2$ particles were observed in the SEM image, and $Ca_{10}(PO_4)_6F_2$ crystals after adsorption could be observed through XRD. When Fe^{2+} and Mn^{2+} exist in solution, Mg^{2+} in $Mg_3Si_2(OH)_4O_5$ ($V = 364.1$) is replaced by Fe^{2+} and Mn^{2+} due to ion exchange; $Fe_3Si_2(OH)_4O_5$ ($V = 391.4$) and $Mn_3Si_2(OH)_4O_5$ ($V = 408.2$) appeared after the reaction. Due to the different cell volumes, fine particles were also formed on the surface of the Srp/HAP composite particles after adsorption of Fe^{2+} and Mn^{2+}. Through XRD analysis, $Fe_3Si_2(OH)_4O_5$ and $Mn_3Si_2(OH)_4O_5$ crystals formed after the adsorption of Fe^{2+} and Mn^{2+} were observed.

The Srp/HAP composite particles adsorbed Fe^{2+} and Mn^{2+}. In addition to undergoing physical adsorption and ion exchange, PO_4^{3-} on the HAP crystal surface may complex with Fe^{2+} and

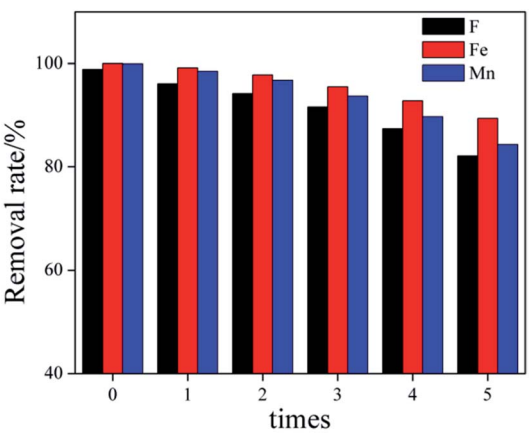

Fig. 15 Regeneration behaviors of the Srp/HAP by 0.1 M Na_2CO_3 and 0.1 M HNO_3.

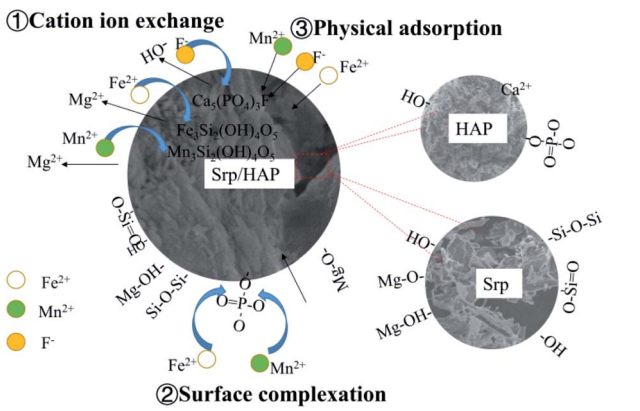

Fig. 16 Schematic diagram of the Srp/HAP adsorption mechanism for F^-, Fe^{2+} and Mn^{2+}.

Mn^{2+}. Bogya *et al.*[45] studied the effect of HAP on Cd^{2+} adsorption and showed that PO_4^{3-} on the surface of the adsorbent adsorbed Cd^{2+} ions by surface complexation. Mavropoulos *et al.*[46] studied the adsorption process of Pb^{2+} by HAP. The results showed that ion exchange alone was not enough to explain the adsorption mechanism of HAP for heavy metal ions, and the authors even speculated that surface complexation might be involved in the whole process of HAP adsorption of heavy metal ions. We found from FTIR analysis that the O–P–O absorption peak weakened, which further confirmed that PO_4^{3-} underwent surface complexation with Fe^{2+} and Mn^{2+}.

Based on the microscopic characterization results, the adsorption of F^-, Fe^{2+} and Mn^{2+} in groundwater by Srp/HAP composite particles involves both physical adsorption and chemical adsorption. Chemical adsorption is mainly manifested as ion exchange or may include surface complexation (Fig. 16).

4. Conclusion

(1) The synthesized Srp/HAP composite has good adsorption properties for F^-, Fe^{2+} and Mn^{2+}, and can be easily regenerated. The optimal preparation conditions were as follows: solid–liquid ratio of Srp to calcium nitrate solution of 20%, aging time of 20 h, calcination temperature of 180 °C, and calcination time of 90 min.

(2) The SEM, EDS, XRD, BET and FT-IR microscopic characterization results show that the newly prepared Srp/HAP adsorbent had compact particles, which not only had a sheet-like curl structure on the Srp surface but also solved the problem of HAP surface agglomeration. After loading, the particle crystals grew compactly and irregularly, the number of surface pores increased, and the number of adsorption sites increased. The specific surface area and pore volume of the composite particle adsorbent were significantly increased compared with those of Srp and HAP, and the surface pore structure was better, which was beneficial to the simultaneous adsorption and removal of fluorine, iron and manganese. The adsorption process includes not only surface physical adsorption but also chemical adsorption, including ion exchange and surface complexation.

(3) The optimal conditions for Srp/HAP treatment of composite water samples with F^-, Fe^{2+} and Mn^{2+} mass concentrations of 5 mg L^{-1}, 20 mg L^{-1} and 5 mg L^{-1} were as follows: dosage of 3 g L^{-1}, pH of 7, reaction temperature of 35 °C, and reaction time of 150 min. Under these conditions, the removal rates of F^-, Fe^{2+} and Mn^{2+} were 98.6%, 99.9%, and 99.8%, respectively.

(4) The experimental adsorption kinetics results showed that the adsorption of F^-, Fe^{2+} and Mn^{2+} ions on Srp/HAP conformed to the quasi-second-order kinetic model and the internal diffusion model. The isotherm data of the adsorption process conformed to the Langmuir isothermal adsorption model. At 35 °C, the maximum monolayer saturated adsorption capacity Q values of F^-, Fe^{2+} and Mn^{2+} by Srp/HAP were 6.2406 mg g^{-1}, 11.9432 mg g^{-1}, and 9.6441 mg g^{-1}, respectively.

(5) This study only considers one method to regenerate the Srp/HAP adsorbent, and it is necessary to further explore the influence of other regeneration methods on the adsorption performance and availability of the adsorbent. In addition, the water used in this test is simulated groundwater sample, and the influence of complex environmental conditions is not considered. In the future, the effects of groundwater chemical types and coexisting ions on the adsorption of F^-, Fe^{2+} and Mn^{2+} by Srp/HAP should be further studied, so as to create conditions for the application of Srp/HAP adsorbents in practical engineering.

Author contributions

All of the authors contributed significantly to this research. Xilin Li: Conceptualization, methodology, writing – reviewing and editing, funding acquisition; Xiaowan Yu: validation, formal analysis, writing – original draft preparation; Ling Liu: resources, project administration, funding acquisition; Jianlin Yang: visualization, supervision; Siyuan Liu: investigation, data curation; Tianyi Zhang: software.

Conflicts of interest

The authors declare that they have no conflicts of interest to report regarding the present study.

Acknowledgements

This work was supported by the National Key R&D Program of China (No. 2017YFC1503106), Liaoning BaiQianWan Talents Program of China (No. 2018C01) and Liaoning Provincial Natural Science Foundation of China (No. 2019-ZD-0037).

References

1 C. Zhu, S. Wang, K. M. Hu, W. X. Wang, A. J. Cai, W. J. Chang and B. Li, Study on fluoride, iron and manganese removal from aqueous solutions by a novel composite adsorbent, *Adv. Mater. Res.*, 2013, **2735**, 1085–1092.

2 L. M. Fan and X. D. Ma, A review on investigation of water-preserved coal mining in western China, *Int. J. Coal Sci. Technol.*, 2018, **5**, 411–416.

3 X. L. Li, M. Fan, L. Liu, J. H. Chang and J. W. Zhang, Treatment of high-concentration chromium-containing wastewater by sulfate-reducing bacteria acclimated with ethanol, *Water Sci. Technol.*, 2019, **80**, 2362–2372.

4 P. Wu, J. S. Wu, L. Xia, Y. Liu, L. Y. Xu and S. X. Song, Adsorption of fluoride at the interface of water with calcined magnesium –ferri–lanthanum hydrotalcite-like compound, *RSC Adv.*, 2017, **7**, 26104–26112.

5 S. Indah, D. Helard and A. Binuwara, Studies on desorption and regeneration of natural pumice for iron removal from aqueous solution, *Water Sci. Technol.*, 2018, **2017**, 509–515.

6 P. Roccaro, C. Barone, G. Mancini and F. G. A. Vagliasindi, Removal of manganese from water supplies intended for

human consumption: a case study, *Desalination*, 2006, **210**, 205–214.

7 M. Mobarak, E. A. Mohamed, A. Q. Selim, L. Sellaoui, A. B. Lamine, A. Erto, A. Bonilla-Petriciolet and M. K. Seliem, Surfactant–modified serpentine for fluoride and Cr (VI) adsorption in single and binary systems: Experimental studies and theoretical modelling, *Chem. Eng. J.*, 2019, **369**, 333–343.

8 M. A. Shavandi, Z. Haddadian, M. H. S. Ismail, N. Abdullah and Z. Z. Abidin, Removal of Fe(III), Mn(II) and Zn(II) from palm oil mill effluent (POME) by natural zeolite, *J. Taiwan Inst. Chem. Eng.*, 2012, **43**, 750–759.

9 S. Mohan, V. Kumar, D. Kumar Singh and S. H. Hasan, Synthesis and characterization of rGO/ZrO_2 nanocomposite for enhanced removal of fluoride from water: kinetics, isotherm, and thermodynamic modeling and its adsorption mechanism, *RSC Adv.*, 2020, **10**, 16791–16803.

10 A. M. Muliwa, T. Y. Leswifi, A. Maity, A. Ochieng and M. S. Onyango, Fixed-bed operation for manganese removal from water using chitosan/bentonite/MnO composite beads, *Environ. Sci. Pollut. Res.*, 2018, **25**, 18081–18095.

11 E. K. Marwa, S. Hassan and H. Hesham, Effect of superparamagnetic nanoparticles on the physicochemical properties of nano hydroxyapatite for groundwater treatment: Adsorption mechanism of Fe(II) and Mn (II), *RSC Adv.*, 2016, **6**, 82244–82259.

12 N. A. Akbar, H. A. Aziz and M. N. Adlan, Iron and Manganese Removal from Groundwater Using High Quality Limestone, *Appl. Mech. Mater.*, 2015, **4197**, 460–465.

13 G. Biswas, M. Kumari, K. Adhikari and S. Dutta, A Critical Review on Occurrence of Fluoride and Its Removal through Adsorption with an Emphasis on Natural Minerals, *Curr. Pollut. Rep.*, 2017, **3**, 104–119.

14 G. T. M. Kadja and M. M. Ilmi, Indonesia natural mineral for heavy metal adsorption: a review, *Journal of Environmental Science and Sustainable Development*, 2019, **2**, 139–164.

15 M. Wang, A. A. Orr, J. M. Jakubowski, K. E. Bird, C. M. Casey, S. E. Hearon, P. Tamamis and T. D. Phillips, Enhanced adsorption of per- and polyfluoroalkyl substances (PFAS) by edible, nutrient-amended montmorillonite clays, *Water Res.*, 2021, **188**, 116534.

16 J. I. Lee, S. H. Hong, C. G. Lee and S. J. Park, Experimental and model study for fluoride removal by thermally activated sepiolite, *Chemosphere*, 2020, **241**, 1–10.

17 C. Tan, H. Xu, D. Cui, J. Zuo, J. Li, Y. Ji, S. Qiu, L. Yao, Y. Chen and Y. Liu, Effects of tourmaline on nitrogen removal performance and biofilm structures in the sequencing batch biofilm reactor, *J. Environ. Sci.*, 2018, **67**, 127–135.

18 M. Wang, K. Zhang, M. Wu, Q. Wu, J. Liu, J. Yang and J. Zhang, Unexpectedly high adsorption capacity of esterified hydroxyapatite for heavy metal removal, *Langmuir*, 2019, **35**, 16111–16119.

19 T. Suzuki, T. Hatsushika and Y. Hayakawa, Synthetic hydroxyapatites employed as inorganic cation-exchangers, *J. Chem. Soc., Faraday Trans. 1*, 1981, **77**, 1059–1062.

20 J. Reichert and J. G. P. Binner, An evaluation of hydroxyapatite-based filters for removal of heavy metal ions from aqueous solutions, *J. Mater. Sci.*, 1996, **31**, 1231–1241.

21 K. Nonaka, A. Iizuka, A. Yamasaki and Y. Yanagisawa, Preparation of Hydroxyapaptite (HAP) from Concrete Sludge and Evaluation of Its Capacity to Remove Cadmium, Copper and Fluoride Ions, *Kagaku Kogaku Ronbunshu*, 2010, **36**, 539–544.

22 J. Y. He, K. Chen, X. G. Cai, Y. L. Li, C. M. Wang, K. S. Zhang, Z. Jin, F. L. Meng, X. G. Wang, L. T. Kong and J. H. Liu, A biocompatible and novelly-defined Al-HAP adsorption membrane for highly effective removal of fluoride from drinking water, *J. Colloid Interface Sci.*, 2017, **490**, 97–107.

23 L. Chen, K. S. Zhang, J. Y. He, W. H. Xu, X. J. Huang and J. H. Liu, Enhanced fluoride removal from water by sulfate-doped hydroxyapatite hierarchical hollow microspheres, *Chem. Eng. J.*, 2016, **285**, 616–624.

24 L. Gong and L. Feng, Preparation and defluorination mechanism of a novel copolymerized hydroxyapatite–aluminium chloride material, *RSC Adv.*, 2015, **5**, 95334–95343.

25 M. Ersan, U. A. Guler, U. Acıkel and M. Sarioglu, Synthesis of hydroxyapatite/clay and hydroxyapatite/pumice composites for tetracycline removal from aqueous solutions, *Process Saf. Environ. Prot.*, 2015, **96**, 22–32.

26 G. Liu, Z. K. Li, L. S. Xu, X. F. Xu, Q. Q. Huang, Y. Zeng and M. Y. Wen, The dynamics and adsorption of Cd (II) onto hydroxyapatite attapulgite composites from aqueous solution, *J. Sol-Gel Sci. Technol.*, 2018, **87**, 269–284.

27 G. J. Li, P. Zhao and Z. M. Bai, Surface Characteristics of Serpentine, *J. Chin. Ceram. Soc.*, 2017, **45**, 1204–1210.

28 X. L. Li, X. W. Yu, L. Li, L. G. Wang and S. Y. Liu, Dynamic adsorption of fluoride, iron and manganese in underground water of mining area by Srp/HAP, *J. China Coal Soc.*, 2020, **46**, 1–11.

29 X. L. Li, F. F. Shang, D. Q. Chen, J. Sun, Z. Hou, B. L. Sun and C. Wang, Experimental study on adsorption of fluoride groundwater by serpentine, *Non-Met. Mines*, 2017, **40**, 86–88.

30 C. S. Sundaram, N. Viswanathan and S. Meenakshi, Uptake of fluoride by nano-hydroxyapatite/chitosan, a bioinorganic composite, *Bioresour. Technol.*, 2008, **99**, 8226–8230.

31 X. Han, Y. Zhang, L. Y. Li, Y. Zhang, R. M. Han, G. X. Wang and W. Wei, Nanosized hydroxyapatite supported on natural sepiolite: A novel adsorbent for Cd(II) removal from simulated groundwater, *Mater. Res. Express*, 2019, **6**, 125518.

32 H. Li, *Study on the preparation of ceramic-coat with the serpentine*, China University of Geosciences, Beijing, 2016.

33 V. Dhand, K. Y. Rhee and S. J. Park, The facile and low temperature synthesis of nanophase hydroxyapatite crystals using wet chemistry, *Mater. Sci. Eng., C*, 2014, **36**, 152–159.

34 H. He, Z. Q. Zhu, J. Liu, Y. N. Zhu, Q. M. Yan, Y. Liu, N. Mo, H. L. Xuan and W. Y. Wei, Removal of Pb^{2+} from aqueous solution by magnesium-calcium hydroxyapatite adsorbent, *Environ. Sci.*, 2019, **40**, 4081–4090.

35 S. Annida, I. Inayat and F. Setiawati, Chromium Metal Biosorption Using Peanut Shell Adsorbent, *Equilibrium Journal of Chemical Engineering*, 2018, **2**, 7–15.

36 K. Q. Li, Z. Zheng, J. C. Jiang and J. B. Zhang, Adsorption Kinetic and Thermodynamic Studies of Lead onto Activated Carbons from Cotton Stalk, *Environ. Sci.*, 2010, **31**, 1402–1408.

37 M. H. Dehghani, M. Faraji, A. Mohammadi and H. Kamani, Optimization of fluoride adsorption onto natural and modified pumice using response surface methodology: Isotherm, kinetic and thermodynamic studies, *Korean J. Chem. Eng.*, 2017, **34**, 454–462.

38 M. Mourabet, A. E. Rhilassi, H. E. Boujaady, M. B. Ziatni, R. E. Hamri and A. Taitai, Removal of fluoride from aqueous solution by adsorption on hydroxyapatite (HAp) using response surface methodology, *J. Saudi Chem. Soc.*, 2015, **19**, 603–615.

39 N. Z. Alias, N. A. M. Zuki, S. H. Alias and M. L. Kamal, Removal of Iron (Fe) by Adsorption using Activated Carbon Moringa oleifera (ACMO) in Aqueous Solution, *Jurnal Intelek*, 2012, **7**, 22–29.

40 M. K. Doula, Removal of Mn^{2+} ions from drinking water by using Clinoptilolite and a Clinoptilolite-Fe oxide system, *Water Res.*, 2006, **40**, 3167–3176.

41 A. B. Jusoh, W. H. Cheng, W. M. Low, A. Nora'aini and M. J. Megat Mohd Noor, Study on the removal of iron and manganese in groundwater by granular activated carbon, *Desalination*, 2005, **182**, 347–353.

42 M. A. Shavandi, Z. Haddadian, M. H. S. Ismail, N. Abdullah and Z. Z. Abidin, Removal of Fe(III), Mn(II) and Zn(II) from palm oil mill effluent (POME) by natural zeolite, *J. Taiwan Inst. Chem. Eng.*, 2012, **43**, 750–759.

43 L. Huang, S. Yuan, L. Lv, G. Tan, B. Liang and S. Pehkonen, Poly(methacrylic acid)-grafted chitosan microspheres *via* surface-initiated ATRP for enhanced removal of Cd (II) ions from aqueous solution, *Colloid Interface Sci.*, 2013, **405**, 171–182.

44 M. Jiménez-Reyes and M. Solache-Ríos, Sorption behavior of fluoride ions from aqueous solutions by hydroxyapatite, *J. Hazard. Mater.*, 2010, **180**, 297–302.

45 E. S. Bogya, C. Melinda, R. Barabás and A. C. Alexandra, Influence of synthesis method of nano-hydroxyapatite-based materials on cadmium sorption processes, *J. Iran. Chem. Soc.*, 2014, **11**, 53–68.

46 E. Mavropoulos, A. M. Rossi, A. M. Costa, C. A. C. Perez, J. C. Moreira and M. Saldanha, Studies on the mechanisms of lead immobilization by hydroxyapatite, *Environ. Sci. Technol.*, 2002, **36**, 1625–1629.